

Journal of Materials Chemistry A

Accepted Manuscript



This is an *Accepted Manuscript*, which has been through the Royal Society of Chemistry peer review process and has been accepted for publication.

Accepted Manuscripts are published online shortly after acceptance, before technical editing, formatting and proof reading. Using this free service, authors can make their results available to the community, in citable form, before we publish the edited article. We will replace this *Accepted Manuscript* with the edited and formatted *Advance Article* as soon as it is available.

You can find more information about *Accepted Manuscripts* in the [Information for Authors](#).

Please note that technical editing may introduce minor changes to the text and/or graphics, which may alter content. The journal's standard [Terms & Conditions](#) and the [Ethical guidelines](#) still apply. In no event shall the Royal Society of Chemistry be held responsible for any errors or omissions in this *Accepted Manuscript* or any consequences arising from the use of any information it contains.

Cite this: DOI: 10.1039/c0xx00000x

www.rsc.org/xxxxxx

ARTICLE TYPE

Expeditious Fabrication of Flower-like Hierarchical Mesoporous Carbon Superstructures as Supercapacitor Electrode Materials

Jiyuan Liang, Shenglan Chen, Mingjiang Xie, Yongzheng Wang, Xiangke Guo, Xuefeng Guo* and Weiping Ding*

5 Received (in XXX, XXX) Xth XXXXXXXXXX 20XX, Accepted Xth XXXXXXXXXX 20XX
DOI: 10.1039/b000000x

We report a facile and efficient strategy for preparing flower-like hierarchical mesoporous carbon superstructures (FMCS) through a one-pot hydrothermal reaction of nickel acetate with glucose. In the fabrication process of FMCS, the nickel acetate ingeniously plays multifunctional roles: as inducer of flower-like hierarchical carbon, as catalyst of graphitization, and as pore-forming agent. First, flower-like Ni(OH)₂/polysaccharide microspheres were self-assembled via the hydrothermal reaction at 180 °C for 24 h. Second, flower-like mesoporous carbon superstructures were obtained by etching and removing the Ni from the Ni/C precursor carbonized from the Ni(OH)₂/polysaccharide microspheres. The obtained flower-like superstructures is composed of two-dimensional mesoporous carbon petal building blocks, with thickness of 20 nm. Electrochemical data showed that the product FMCS-1 displayed a specific capacitance of 226 F/g at 0.5 A/g, and retained 82% (185 F/g) at high current density of 20 A/g, indicative of outstanding rate capability. Furthermore, the three-dimensional (3D) flower-like hierarchical mesoporous carbon superstructures demonstrated excellent cycle stability with approximately 100% retention of initial specific capacitance after 2000 cycles at current density of 10 A/g.

1. Introduction

Due to the fast consumption of non-renewable fossil energy, human being begins to seek new energy, e.g. solar and wind energy, in order to satisfy the increasing demand. However, the productions of these energies are not even and continuous. Hence, high-performance energy storage devices are needed to store the generated energy.¹ Among these energy storage devices, supercapacitor is a promising candidate because it has higher power density than batteries, and higher energy density than conventional capacitors.² In general, supercapacitors can be classified into two categories, namely, the electrical double-layer capacitors (EDLCs), with carbon-based materials as active materials, and the Faradaic pseudocapacitors, with transition metal oxides (RuO₂, Co₃O₄, MnO₂, NiO, etc.) and hydroxides (Ni(OH)₂, Co(OH)₂, etc.), or conducting polymers as active materials.³⁻⁸

Among various electrode materials, porous carbon-based materials have attracted great interest due to their high surface area, good electrical conductivity, high chemical/thermal stability and low cost.^{9, 10} During the past decades, porous carbons with micro or mesoporous structures have been widely studied as electrode materials for supercapacitors.¹¹⁻¹⁵ The previous investigations clearly show that the structures of porous carbons have an important influence on their performances. Microporous carbon materials, for example, activated carbons, have high surface areas with random pore distribution including micropores

smaller than 1 nm and a long diffusion distance, which could storage much more charges at low current density, but leads to low accessible surfaces area at high current density.^{16, 17} Hence, their applications are restricted due to the limited energy storage and rate capability. Compared with microporous carbon, mesoporous carbon has larger pore size, which is expected to favor fast electrolyte ions transport in the bulk, leading to a good rate performance.¹⁸⁻²² However, mesoporous carbons have lower specific surface areas than that of microporous carbons, so they usually have a low capacitance even at low current density. Recently, the design and synthesis of three dimensional (3D) hierarchical porous carbon materials consisting of interconnected micropores, mesopores and macropores are of great interest due to their hierarchical pores and structural diversity and their potential applications in catalysis, separation, advanced functional materials, etc.²³⁻²⁶ Among them, 3D flower-like hierarchical porous carbon material has attracted special attention due to their unique carbon sheets and the high specific surface area and excellent interconnected pore structure. Compared with microporous carbon and mesoporous carbon, 3D flower-like hierarchical porous carbon not only has a high accessible surface area for electrolytes, but also facilitates electrolyte ions transport by shortening the diffusion distance.^{27, 28} Up to date, only few approaches have been reported for the successful synthesis of 3D flower-like hierarchical porous carbon, which mainly involves the use of complicated template and the tedious multi-step and costly process. For example, very recently, Wang *et al.* reported a 3D flower-like hierarchical porous carbon material fabricated

through a carbonization method followed by chemical activation with a pre-prepared flower-like ZnO as template and pitch as carbon precursor.²⁹ Until now, to fabricate 3D flower-like porous carbon superstructures through a simple approach has remained a challenge.

Herein, we report a convenient strategy for the synthesis of 3D flower-like mesoporous carbon superstructures (FMCS) through a one-pot hydrothermal reaction and carbonization processes without any additional template. The preparation scheme was shown in Fig. 1. In the fabrication process of FMCS, the nickel acetate is used for multiple purposes: as inducer of flower-like hierarchical carbon, as catalyst of graphitization, and as pore-forming agent. The obtained 3D FMCS is composed by 2D carbon nanosheets with mesopores, which could provide large accessible active sites for electrical charge storage. The graphitic pores in the carbon sheets formed conductive network which will enhance the electrons transfer. The 3D FMCS-based electrodes exhibit outstanding super-capacitive performances and rate capability, indicating potential applications as high-rate supercapacitor electrode materials. This study also provides a new insight into the rational design of 3D hierarchical porous carbons as electrode materials for energy storage applications.

2. Experimental

2.1. Synthesis of FMCS and carbon sphere

All reagents were pure and thus were used without purification. In a typical synthesis procedure of FMCS-1, as shown in Fig. 1, firstly, 2.48 g $\text{Ni}(\text{CH}_3\text{COO})_2 \cdot 4\text{H}_2\text{O}$ and 0.98 g glucose (1.98 g for FMCS-2), were dissolved in 35.0 mL distilled water. The solution was then transferred into a 50.0 mL Teflon-lined stainless steel autoclave, which was then sealed and kept in an oven of 180 °C for 24 h. After cooling down to room temperature, the precipitate was collected and subsequently washed with distilled water before it was dried in an electric oven at 70 °C. Secondly, the dried product was calcined at 700 °C under Ar for 3 h with a ramp rate of 2 °C/min and the product was transformed into Ni/C composite. Finally, Ni particles in Ni/C composite were removed by hydrothermal treatment in HCl (37 wt %) solution at 180 °C for 24 h. The final product (FMCS) was centrifuged, washed with distilled water and ethanol, and dried at 70 °C in air. For comparison, carbon spheres were synthesized with the same procedure, but without using nickel acetate in the hydrothermal reaction. Briefly, 35.0 mL solution containing 1.98 g glucose was hydrothermally treated at 180 °C for 24 h, the resulted solids was centrifuged, washed with distilled water and ethanol, and calcined at 700 °C under Ar for 3 h.

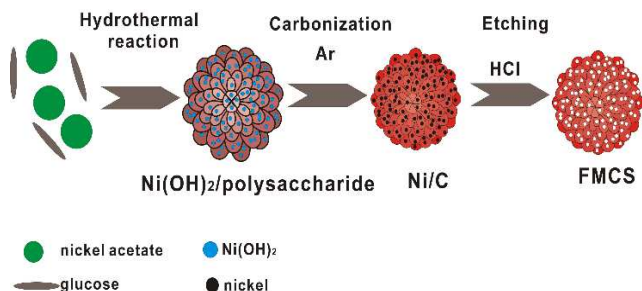


Fig. 1 Schematic illustration of the preparation of 3D FMCS.

2.2. Characterization

The morphology and structure were examined by scanning electron microscope (SEM, Hitachi S-4800) and transmission electron microscope (TEM, JEOL-2011). The crystal phases were identified by wide-angle X-ray powder diffraction (XRD) and the patterns were recorded on Philips X' Pro diffract meter using $\text{Cu K}\alpha$ radiation ($\lambda = 1.5418 \text{ \AA}$) at 40 kV and 40 mA. Thermogravimetric (TG) was performed in NETZSCH STA 449 C at a heating rate of 5 °C/min from room temperature to 800 °C in an Al_2O_3 sample pan. Raman spectra were measured by a Horiba LabRAM Aramis Raman system with a 514 nm laser as the excitation source. The specific surface area was determined by N_2 sorption at -196 °C using an adsorption apparatus (Micromeritics Tristar 3020), with the adsorption data fitted to the Brunauer-Emmett-Teller (BET) equation. The pore size distribution was derived from the desorption branches of the isotherms by means of Barrett-Joyner-Halenda (BJH) method.

2.3. Electrochemical tests

Electrochemical tests were performed in a three-electrode glass cell in 6.0 M KOH solution at room temperature. The working electrode was prepared by mixing the as-prepared samples, acetylene black, and poly(tetrafluoroethylene) (PTFE) binder with a weight ratio of 80:15:5, which were pressed (10 MPa) onto a nickel foam and dried in an vacuum oven at 80 °C for 12 h. A platinum wire and an Hg/HgO electrode were used as counter and reference electrodes, respectively. All the electrochemical tests were carried out on a CHI660D electrochemical workstation (CH Instruments Inc.). The cyclic voltammetry (CV) experiments were performed between -1 and 0 V at a scan rate of 10~200 mV/s. The galvanostatic charge-discharge (CD) behaviour was investigated within the potential window -1 V~0 V at various current densities. The specific capacitance can be calculated by $C = It/m\Delta V$, where I is the discharge current, t is the discharge time, m is the mass of the active materials, ΔV is the voltage drop upon discharging. Electrochemical impedance spectroscopy (EIS) tests were carried out with a frequency loop from 10^5 Hz to 0.01 Hz using perturbation amplitude of 5 mV at open circuit voltage.

3. Results and discussion

The products of hydrothermal reaction were imaged by SEM and TEM. As shown in Fig. 2a, uniform flower-like spheric solids with diameter size of 2-5 μm could be formed after hydrothermal reaction. Only carbon spheres (Fig. S1) can be obtained without nickel acetate. The flower-like precursor was composed of very thin two-dimensional carbon petals with thickness of 20 ~ 30 nm (Fig. 2b). HRTEM image (Fig. 2d) of the edge of carbon nanosheet showed that many well dispersed nanoparticles embedded in the carbon sheets and their diameter was about 5 nm. The interplanar spacing of the nanoparticle is 0.397 nm (inset of Fig.2d), which corresponds to the d spacing of (006) plane of $\alpha\text{-Ni}(\text{OH})_2$. In order to further confirm the composition of those nanoparticles, the precursor was tested by XRD. The XRD pattern (Fig. 3a) clearly shows that these nanoparticles are $\alpha\text{-Ni}(\text{OH})_2$ particles and there are no additional impurity diffraction from the precursors. Since glucose is easy to be hydrothermally polymerized into polysaccharide (carbon-rich), the XRD results suggested that the precursor was composed of

α -Ni(OH)₂ nanoparticles and polysaccharide. The possible formation mechanism could be described as follows. Firstly, amorphous Ni(OH)₂ is formed due to the forced hydrolysis of nickel acetate (Ni(Ac)₂) at high temperature and self-assembled into petals. The reaction is illustrated below:



Meanwhile, glucose might be adsorbed on the surface of Ni(OH)₂ due to the hydrogen-bonding interaction, and was hydrothermally polymerized into polysaccharide and was coated on the surface of Ni(OH)₂. Along with the prolonged hydrothermal process, the amorphous Ni(OH)₂ petals might crystallized into α -Ni(OH)₂ nanoparticles with the coating of polysaccharide.

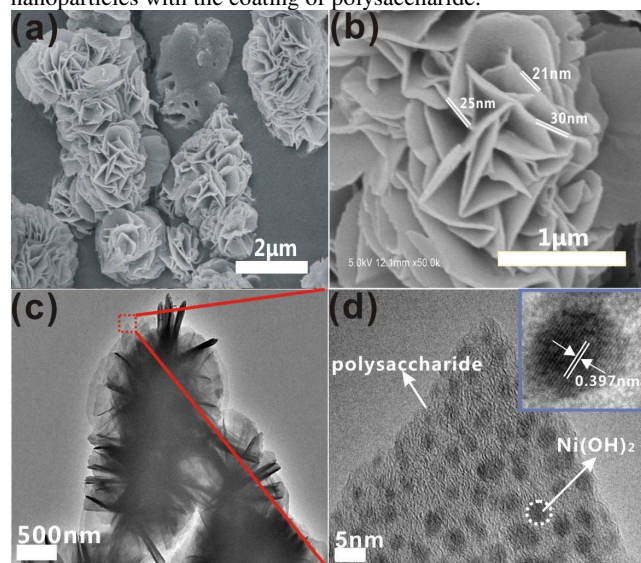


Fig. 2 (a,b) SEM, (c)TEM and (d)HRTEM images of the product of hydrothermal reaction.

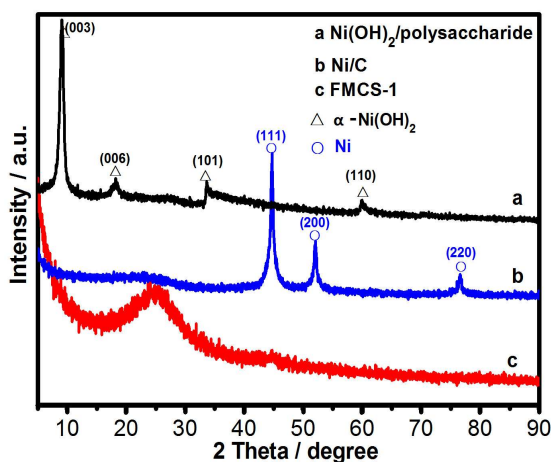


Fig. 3 XRD patterns of (a) Ni(OH)₂/polysaccharide precursor, (b) Ni/C composite and (c) FMCS-1.

As shown in Fig. 4a, SEM images of the obtained Ni/C composite showed that the flower-like structure could be well-maintained after calcination/carbonization of Ni(OH)₂/polysaccharide composite under Ar atmosphere. While the surface of nanosheets became rough due to the shrinkage of polysaccharide during the carbonization process. The thickness of the carbon petals was reduced to about 20 nm (Fig. 4b). The

corresponding XRD pattern was shown in Fig. 3b, there were three obvious diffraction peaks at 44.5°, 51.8° and 76.4° emerged, which could be attributed to be the (111), (200) and (220) diffractions of cubic Ni (JCPDS: No.04-0850). It's well known that the polysaccharide will be carbonized at 700°C under Ar, the XRD results confirmed that the obtained composites would be Ni/C composites. Fig. 4c showed the typical TEM image of Ni/C composite. It can be seen that some big Ni particles with size of ~50 nm emerged in the carbon nanosheets. Enlarged TEM images (Fig. 4d) from the edge of sheets clearly demonstrated that there were a lot of small Ni particles with size of ~4 nm homogeneously embed in the 2D carbon nanosheet. The interplanar spacing is 0.201 nm (inset of Fig.4d), which is in good agreement with the *d* spacing of (111) plane of cubic Ni. Compared with the corresponding Ni(OH)₂/polysaccharide precursor, it's obvious that the small Ni nanoparticles are derived from the ~5 nm α -Ni(OH)₂ nanoparticles because of the reduction of α -Ni(OH)₂ to Ni during the carbonization process. The big Ni particles maybe formed by the agglomeration of some small Ni nanoparticles with less polysaccharide coating under high temperature.

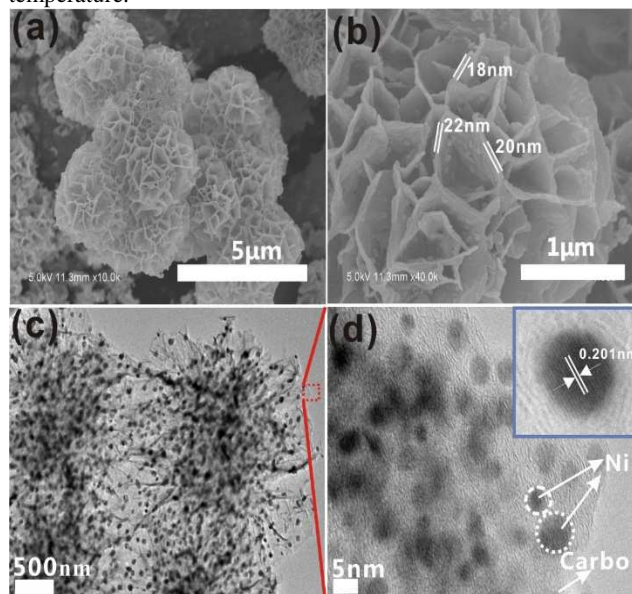


Fig. 4 (a,b) SEM, (c) TEM and (d) HRTEM images of Ni/C composites.

In order to obtain the 3D FMCS, the Ni/C composites were etched in HCl solution. After acid treatment, the diffraction peaks of Ni particles disappeared (Fig. 3c), indicating that the effective removal of Ni nanoparticles. The broadened peak near 25° which could be attributed to the (002) diffraction peak of graphite, indicated that there were short-range order crystal structure existed in the obtained carbon material.³¹ Fig. 5a showed the SEM image of the obtained FMCS-1. After calcining and etching processes, the original flower-like carbon morphology can be well maintained and the obtained uniform flower-like carbon spheres FMCS-1 have diameters ranging from 2 to 5 μm. TEM measurements were carried out to further investigate the structure of the as-synthesized 3D hierarchical mesoporous carbons spheres. Fig. 5b showed that FMCS-1 have hollow structure. HRTEM image of FMCS-1 clearly revealed that the porous carbon presents an onion-like carbon shells within the carbon

sheets. The lattice fringes of the onion-like carbon shells showed an interplanar spacing of 0.346 nm, which could be attributed to graphitic (002) layers, suggesting the graphitic carbon shells (Fig. 5d).³² The SEM and TEM images of FMCS-2 (Fig. S2) were similar to that of FMCS-1, except the thicker nanosheets of FMCS-2 due to the more glucose in the synthesis.

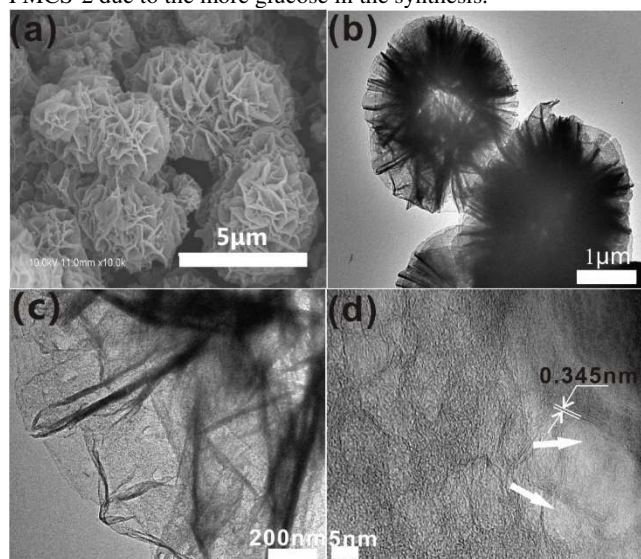


Fig. 5 (a) SEM, (b,c) TEM and (d) HRTEM images of FMCS-1. The presence of mesopores is indicated by the white arrows.

The nitrogen adsorption-desorption isotherms were shown in Fig. 6a. Both of the FMCS can be classified as type IV isotherm, according to the International Union of Pure and Applied Chemistry (IUPAC) classification. At a relative pressure of above 0.4, the distinct hysteresis loop reflects the capillary condensation of the mesopores. The nitrogen adsorption-desorption isotherms of carbon sphere (Fig. S3) indicated a tanglesome porous structure. The specific surface areas (S_{BET}) of FMCS-1 and FMCS-2 are calculated to be 796 and 612 m^2/g , respectively. The specific surface area of carbon sphere is 404 m^2/g , lower than that of 3D FMCS. Fig. 6b showed a narrow pore size distribution for both of FMCS with pore size of 3.9 nm, in accordance to the TEM results. The mesopores were derived from the removal of the Ni nanoparticles embedded in the carbon sheet matrix. The mesopore size agreed very well with the Ni nanoparticle size, based on above HRTEM data of the Ni/C composites and FMCS-1 (Fig. 4d and Fig. 5d). TG results (Fig. S4) showed that the last weight of Ni/C composite was 35.5%. However, FMCS-1 was completely combustion after 800 °C in air. The results further illustrated that the obtained 3D hierarchical mesoporous carbon superstructures were clean, and the nickel particles have been completely removed, in accordance to the XRD results.

The obtained 3D hierarchical mesoporous carbon superstructures and carbon sphere were also characterized by Raman spectroscopy. Raman spectrum (Fig. 7) clearly showed two distinguishable peaks at 1340 cm^{-1} (D-band) and 1590 cm^{-1} (G-band). The D-band is associated with disorder, allowing zone edge modes of the graphite structure to become active due to the lack of long-range order in amorphous and quasi-crystalline forms of carbon materials. The G-band corresponds to the E_{2g} mode in the basal plane of the crystalline graphite.³³ The peak intensity ratio between D and G-bands usually provides a useful

index for comparing the degree of crystallinity of carbon materials, that is, the smaller the ratio of I_D/I_G , the higher the degree of ordering in the carbon material.³⁴⁻³⁶ The I_D/I_G ratio for FMCS-1 and FMCS-2 is 0.90 and 0.91, respectively, in accordance to the existence of graphitic carbon shells indicated by TEM results. However, the I_D/I_G ratio of carbon sphere is 1.2, which is larger than that of 3D flower-like hierarchical mesoporous carbon spheres, and demonstrates that carbon sphere has lower degree of graphitization than that of 3D flower-like hierarchical mesoporous carbon spheres.

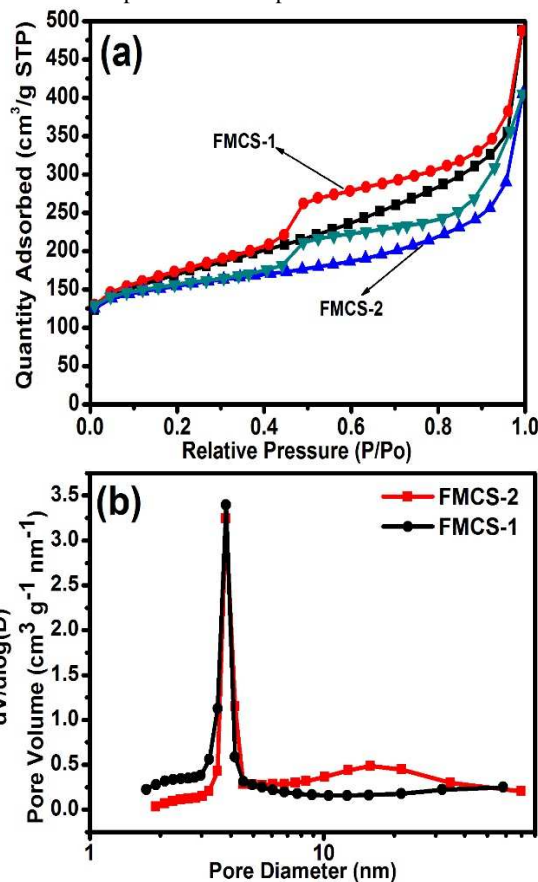


Fig. 6 (a) Nitrogen adsorption-desorption isotherms and (b) pore size distribution curve of the FMCS.

Based all above results, the obtained 3D flower-like hierarchical mesoporous carbon superstructures are composed of 2D carbon nanosheets with mesoporous structure. These results clearly showed that the nickel acetate plays a pivotal role for the fabrication of FMCS with multiple functions: inducing the formation of flower-like hierarchical precursor, offering catalyst for graphitization, and serving as mesopore template. Only carbon spheres can be obtained without nickel acetate. The channel between carbon nanosheets form macropores, which can serve as ion buffering reservoirs, minimizing the diffusion distance between the electrolyte and the interior pore surface of the carbon sheets.³⁷ Moreover, the 2D carbon nanosheets with mesoporous structure, provide highly accessible pathways for the solvent and ions, can sufficiently contact with the electrolyte and facilitate fast adsorption of electrical charge. The stacked graphitic carbon shells may be very beneficial for fast electron transport, thus further enhance the whole electrochemical

performance.

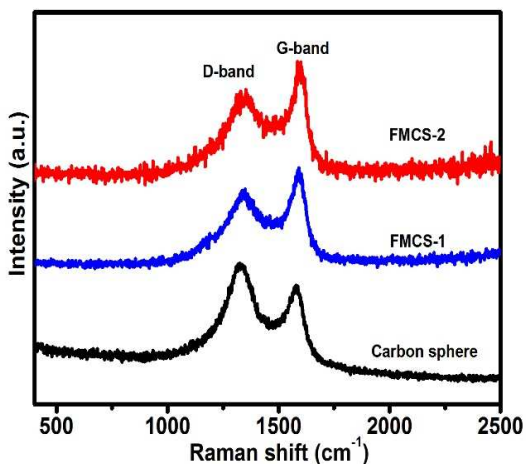


Fig. 7 Raman spectra of 3D FMCS and carbon sphere.

The electrochemical capacitive performances of the obtained carbon materials were performed by CV and CD measurements. Both of the CV curves of FMCS (Fig. 8a and Fig. S5a) display relatively good rectangular profile, showing a typical characteristic of double-layer capacitance. When the scan rate is increased from 10 mV/s to 200 mV/s, a similar rectangular shape is retained, indicating a good capacitive performance at high scan rates for fast electrolyte movement within the electrodes and good charge propagation of ions at the interfaces between the electrolyte and the carbon material. For carbon sphere-based electrode, the CV curve is distorted fiercely even at a low scan rate (Fig. S5c). Under the same electrode preparation and testing conditions, the CV curve of the FMCS-1 based electrode has a larger encircled area than that of FMCS-2 and carbon sphere based electrodes, suggesting that the FMCS-1 based electrode has a better capacitance performance, which may be mainly attributed to its highest specific surface area.

Fig. 8b and Fig. S5b show the CD curves of the FMCS-1 and FMCS-2 based electrodes at various current densities from -1 V to 0 V, respectively. The CD curves at different current densities all show isosceles triangular shapes, suggesting excellent Coulombic efficiency and ideal capacitor behavior. No sudden potential drop is observed, revealing that FMCS based electrochemical electrodes have low equivalent series. By contrast, there is an obvious potential drop in the CD curve of carbon sphere (Fig. S5d). The results further indicated that the nickel acetate not only serves as inducer, but also offer catalyst for the graphitization, which enhances the conductivity. In addition, the discharge time of FMCS-1 is longer than that of FMCS-2 and carbon sphere at the same current density, and thus the specific capacitance of FMCS-1 is higher than that of FMCS-2, in accord with the CV results.

Fig. 9a shows the curves of the specific capacitance vs. current densities for the electrodes made from the synthesized 3D hierarchical mesoporous carbon superstructures and carbon sphere. The specific capacitance of the FMCS-1, FMCS-2 and carbon sphere can be calculated to be 226, 168 and 62 F/g at discharge current density of 0.5 A/g, respectively. Impressively, both of the two hierarchical mesoporous carbon superstructures not only exhibit a much high specific capacitance at 0.5 A/g, but

also maintain them well at higher current densities. When the current density increases to 20 A/g, the specific capacitance of FMCS-1 can still maintain to 185 F/g and preserves 82% of its specific capacitance delivered at 0.5 A/g. FMCS-2 could preserve 80% of its specific capacitance. In contrast, the specific capacitance of carbon sphere decreases sharply with the increasing current density and only retains 37% at the current density of 20 A/g. The high capacitance and excellent rate performance of the hierarchical mesoporous carbon superstructures are mainly attributed to the significantly enhanced accessible surface area and the special hierarchical pore structure.

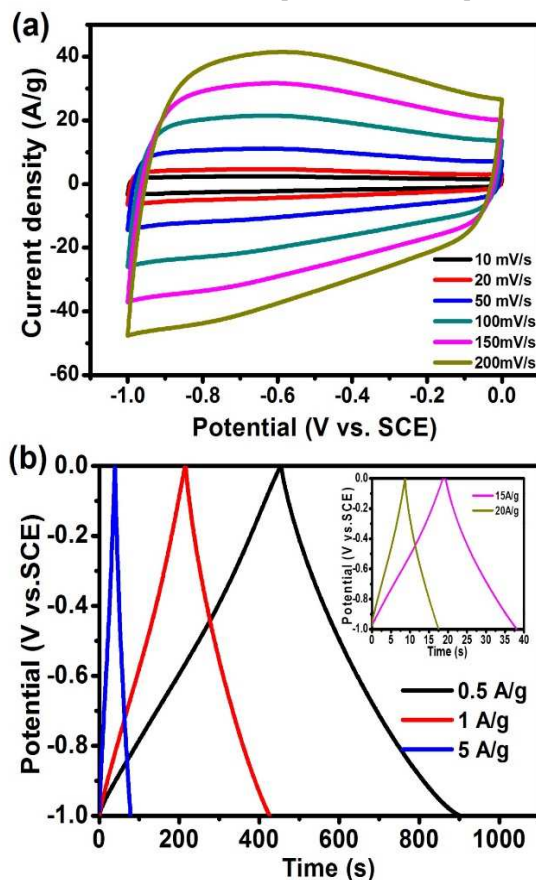
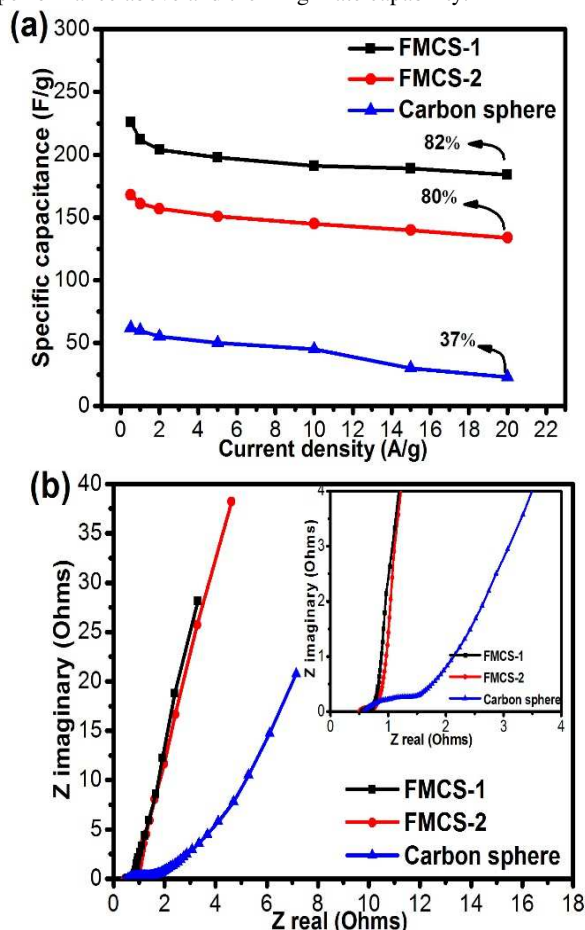


Fig. 8 (a) Cyclic voltammograms of FMCS-1 based electrode at various scan rates. (b) Charge/discharge curves of FMCS-1 based electrode at various current densities.

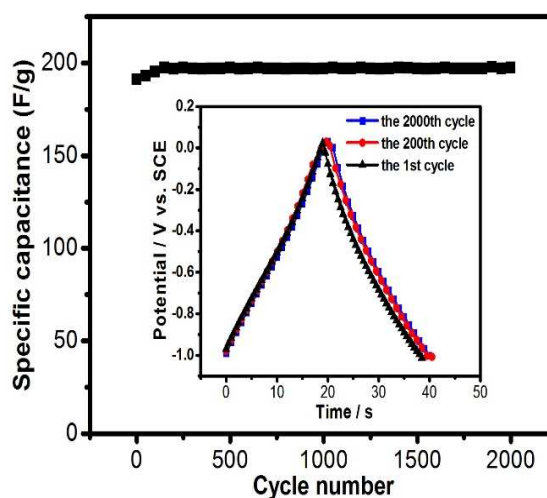
Electrochemical Impedance Spectroscopy (EIS) is a useful method to evaluate the transport property of an electrochemical system. Fig. 9b shows the Nyquist plots of the FMCS-1, FMCS-2 and carbon sphere, respectively. Nyquist plot exhibits two distinct parts including a semicircle in the high frequency region and a sloped line in the low frequency region. In the high frequency region, the semicircle corresponds to the charge-transfer resistance at the electrode/electrolyte interface.^{22, 38} Carbon sphere has the largest charge-transfer resistance. The large resistance of carbon sphere electrode is consequently related to its low electrical conductivity. In contrast, for the FMCS, the added nickel acetate will be transferred into nickel during the calcination process which is a good catalyst for graphitization,³⁹ thus enhances the conductivity of FMCS. In the low frequency region, 3D FMCS has straight line along the imaginary axis,

which demonstrates their low electrolyte ions diffusion resistance and more ideal capacitor behavior.⁴⁰ It can be mainly ascribed to the 3D hierarchical superstructure, which facilitates electrolyte fast contact to the carbon nanosheets and less jammed ion paths.
 5 The low diffusion and electron transfer resistances of the synthesized 3D hierarchical mesoporous carbon superstructures revealed by EIS measurement is consistent with the results of CV performance above and their high rate capability.



10 **Fig. 9** (a) Corresponding specific capacitances of FMCS and carbon sphere at different current densities; (b) Nyquist plots of electrodes based on FMCS and carbon sphere.

15 Stability over repeated charge and discharge cycling is critical for practical application and is demonstrated by continuous charge-discharge cycling test for 2000 cycles. The cycle stability of the synthesized 3D hierarchical mesoporous carbons spheres based electrodes is examined and results are shown in Fig. 10. It
 20 is found that the specific capacitance of FMCS-1 shows a slight increase (103%) after the 200 cycles, which is possibly due to the activation process, which means that unused electrochemically active sites of active material inside the nickel foam electrode are fully exposed to the electrolyte during the cycling process.^{41, 42}
 25 After 2000 cycles at the current density of 10 A/g, the specific capacitance of 3D hierarchical mesoporous carbon spheres electrodes retains 103%. Compared with the charge/discharge curve of the 200th cycle, no obvious changes can be found on
 30 that of the 2000th cycle (Fig.10), illustrating a remarkable cycling stability and life time as electrodes for supercapacitor.



35 **Fig. 10** The cycling performance of FMCS-1 electrodes at the current density of 10 A/g (inset: the charge/discharge curves for the 1st, 200th and 2000th cycles).

35 Based on the above comparison of the carbon sphere and FMCS, it is obvious that the superior electrochemical performance of FMCS electrode is greatly attributed to its unique flower-like hierarchical mesoporous carbon superstructure. As
 40 the basic building blocks, the ultrathin carbon nanopetals with rich mesopores offer the material high accessible surface area for electrolytes, resulting in highly increased capacitance. The special macropores assembled by the ultrathin carbon nanopetals serve as ion-buffering reservoirs, which provide a short diffusion distance and benefit the rapid transport of electrolyte to the inside of the
 45 hierarchical material, leading to its outstanding high rate performance at high current density.^{28,36} And more, the graphitic carbon shells in the FMCS electrode compose an excellent conductive network, which facilitates the transfer of electrons at
 50 high charge/discharge rates, and is beneficial for its rate capability. Due to the outstanding electrochemical performances, the 3D flower-like hierarchical mesoporous carbon superstructures show promising applications as high-rate supercapacitor electrode materials, which also provides new
 55 insight into the rational design of 3D hierarchical porous carbons for energy storage applications.

4. Conclusions

In summary, we have proposed a simple strategy for the synthesis
 60 of 3D flower like mesoporous carbon superstructures through a one-pot hydrothermal reaction and carbonization processes without any additional template. The nickel acetate plays an ingenious and pivotal role for the fabrication of FMCS with
 multiple functions: inducing the formation of flower-like hierarchical precursor, offering catalyst for graphitization, and serving as mesopore template. Electrochemical data demonstrated
 65 that FMCS-1 delivers a specific capacitance 226 F/g at 0.5 A/g and 184 F/g even at a higher current density of 20 A/g with excellent electrochemical stability, suggesting that FMCS would
 70 be a highly promising electrode material for high-rate performance supercapacitors. Such intriguing electrochemical performances are attributed to the 3D interconnected pore texture

and highly accessible mesopores on the ultrathin carbon sheets for efficient electrical charge storage, as well as the excellent conductive network.

Acknowledgments

This work was financially supported by the National Basic Research Program (2009CB623504), the National Science Foundation of China (21173119, 21273109, 21303083), the Natural Science Foundation of Jiangsu Province (SBK201340143), the Specialized Research Fund for the Doctoral Program of Higher Education (20130091120045), Jiangsu Province Innovation for Ph.D Candidate (CX LX13_028) and the Fundamental Research Funds for the Central Universities.

Notes and references

Key Lab of Mesoscopic Chemistry, School of Chemistry and Chemical Engineering, Nanjing University, Nanjing 210093, China. Fax: +86 25 83317761; Tel: +86 25 83686393; E-mail: guoxf@nju.edu.cn, dingwp@nju.edu.cn

† Electronic Supplementary Information (ESI) available: [details of any supplementary information available should be included here]. See DOI: 10.1039/b000000x/

- C. Liu, F. Li, L. P. Ma and H. M. Cheng, *Adv. Mater.*, 2010, **22**, E28-62.
- P. Simon and Y. Gogotsi, *Acc. Chem. Res.*, 2013, **46**, 1094-1103.
- P. Simon and Y. Gogotsi, *Nat. Mater.*, 2008, **7**, 845-853.
- G. P. Wang, L. Zhang and J. J. Zhang, *Chem. Soc. Rev.*, 2012, **41**, 797-828.
- Y. Huang, J. J. Liang and Y. S. Chen, *Small*, 2012, **8**, 1805-1834.
- J. Jiang, Y. Y. Li, J. P. Liu, X. T. Huang, C. Z. Yuan and X. W. Lou, *Adv. Mater.*, 2012, **24**, 5166-5180.
- T. Zhai, F. X. Wang, M. H. Yu, S. L. Xie, C. L. Liang, C. Li, F. M. Xiao, R. H. Tang, Q. X. Wu, X. H. Lu and Y. X. Tong, *Nanoscale*, 2013, **5**, 6790-6796.
- G. Zhang, L. Yu, H. E. Hoster and X. W. Lou, *Nanoscale*, 2013, **5**, 877-881.
- Y. P. Zhai, Y. Q. Dou, D. Y. Zhao, P. F. Fulvio, R. T. Mayes and S. Dai, *Adv. Mater.*, 2011, **23**, 4828-4850.
- X. Li and B. Q. Wei, *Nano Energy*, 2013, **2**, 159-173.
- C. G. Liu, Z. N. Yu, D. Neff, A. Zhamu and B. Z. Jang, *Nano letters*, 2010, **10**, 4863-4868.
- C. X. Guo and C. M. Li, *Energy Environ. Sci.*, 2011, **4**, 4504-4507.
- W. Li, F. Zhang, Y. Q. Dou, Z. X. Wu, H. J. Liu, X. F. Qian, D. Gu, Y. Y. Xia, B. Tu and D. Y. Zhao, *Adv. Energy Mater.*, 2011, **1**, 382-386.
- C. Portet, G. Yushin and Y. Gogotsi, *Carbon*, 2007, **45**, 2511-2518.
- S. Chen, W. Xing, J. Duan, X. Hu and S. Z. Qiao, *J. Mater. Chem. A*, 2013, **1**, 2941-2954.
- E. Frackowiak, *Phys. Chem. Chem. Phys.*, 2007, **9**, 1774-1785.
- D. D. Zhou, Y. J. Du, Y. F. Song, Y. G. Wang, C. X. Wang and Y. Y. Xia, *J. Mater. Chem. A*, 2013, **1**, 1192-1200.
- D. W. Wang, F. Li, M. Liu, G. Q. Lu and H. M. Cheng, *J. Phys. Chem. C*, 2008, **112**, 9950-9955.
- J. Lee, S. Yoon, T. Hyeon, S. M. Oh and K. B. Kim, *Chem. Commun.*, 1999, **21**, 77-2178.
- C. M. Chen, Q. Zhang, C. H. Huang, X. C. Zhao, B. S. Zhang, Q. Q. Kong, M. Z. Wang, Y. G. Yang, R. Cai and D. S. Su, *Chem. Commun.*, 2012, **48**, 7149-7151.
- C. H. Huang, Q. Zhang, T. C. Chou, C. M. Chen, D. S. Su and R. A. Doong, *ChemSusChem*, 2012, **5**, 563-571.
- Y. R. Liang, Z. H. Li, R. W. Fu and D. C. Wu, *J. Mater. Chem. A*, 2013, **1**, 3768-3773.
- Z. S. Wu, S. Yang, Y. Sun, K. Parvez, X. Feng and K. Müllen, *J. Am. Chem. Soc.*, 2012, **134**, 9082-9085.
- L. Qie, W. M. Chen, H. H. Xu, X. Q. Xiong, Y. Jiang, F. Zou, X. L. Hu, Y. Xin, Z. L. Zhang and Y. H. Huang, *Energy Environ. Sci.*, 2013, **6**, 2497-2504.
- X. Cao, Y. Shi, W. Shi, G. Lu, X. Huang, Q. Yan, Q. Zhang and H. Zhang, *Small*, 2011, **7**, 3163-3168.
- F. Xu, R. J. Cai, Q. C. Zeng, C. Zou, D. C. Wu, F. Li, X. E. Lu, Y. R. Liang and R. W. Fu, *J. Mater. Chem.*, 2011, **21**, 1970-1976.
- C. Z. Yuan, B. Gao, L. F. Shen, S. D. Yang, L. Hao, X. J. Lu, F. Zhang, L. J. Zhang and X. G. Zhang, *Nanoscale*, 2011, **3**, 529-545.
- H. Jiang, P. S. Lee and C. Z. Li, *Energy Environ. Sci.*, 2013, **6**, 41-53.
- Q. Wang, J. Yan, Y. B. Wang, T. Wei, M. L. Zhang, X. Y. Jing and Z. J. Fan, *Carbon*, 2014, **67**, 119-127.
- N. Du, Y. F. Chen, C. X. Zhai, H. Zhang and D. R. Yang, *Nanoscale*, 2013, **5**, 4744-4750.
- W. X. Chen, H. Zhang, Y. Q. Huang and W. K. Wang, *J. Mater. Chem.*, 2010, **20**, 4773-4775.
- X. K. Guo, Q. Fan, L. Yu, J. Y. Liang, W. X. Ji, L. M. Peng, X. F. Guo, W. P. Ding and Y. F. Chen, *J. Mater. Chem. A*, 2013, **1**, 11534-11538.
- C. G. Hu, Y. Xiao, Y. Zhao, N. Chen, Z. P. Zhang, M. H. Cao and L. T. Qu, *Nanoscale*, 2013, **5**, 2726-2733.
- S. M. Yoon, W. M. Choi, H. Baik, H. J. Shin, I. Song, M. S. Kwon, J. J. Bae, H. Kim, Y. H. Lee and J. Y. Choi, *ACS Nano*, 2012, **6**, 6803-6811.
- Y. M. Tan, C. F. Xu, G. X. Chen, Z. H. Liu, M. Ma, Q. J. Xie, N. F. Zheng and S. Z. Yao, *ACS Appl. Mater. Interfaces*, 2013, **5**, 2241-2248.
- C. W. Huang, C. H. Hsu, P. L. Kuo, C. T. Hsieh and H. Teng, *Carbon*, 2011, **49**, 895-903.
- D. W. Wang, F. Li, M. Liu, G. Q. Lu and H. M. Cheng, *Angew. Chem., Int. Ed.*, 2008, **47**, 373-376.
- Y. Wang, Z. Q. Shi, Y. Huang, Y. F. Ma, C. Y. Wang, M. M. Chen and Y. S. Chen, *J. Phys. Chem. C*, 2009, **113**, 13103-13107.
- D. Y. Zhai, H. D. Du, B. H. Li, Y. Zhu and F. Y. Kang, *Carbon*, 2011, **49**, 725-729.
- D. Puthusseri, V. Aravindan, S. Madhavi and S. Ogale, *Energy Environ. Sci.*, 2014, **7**, 728-735.
- J. Xu, S. L. Gai, F. He, N. Niu, P. Gao, Y. J. Chen and P. P. Yang, *J. Mater. Chem. A*, 2014, **2**, 1022-1031.
- X. J. Zhang, W. H. Shi, J. X. Zhu, W. Y. Zhao, J. Ma, S. Mhaisalkar, T. L. Maria, Y. H. Yang, H. Zhang, H. H. Hng and Q. Y. Yan, *Nano Res.*, 2010, **3**, 643-652.